Thus, the present strategy efficiently differentiates both mESCs and miPSCs into osteoblasts by sequentially treating the cells with four small molecules, CHIR, Cyc, SAG, and TH, under chemically defined conditions.

Finally, we cultured hiPSCs according to the present strategy with some modifications (Figure 4A; Supplemental Experimental Procedures). hiPSCs formed colonies on day 0. In the mesoderm induction phase, these colonies were disrupted, but the cells generated some clusters upon CHIR and Cyc treatment. The remaining cells proliferated and formed colonies by days 19 and 23 of the osteoblast induction and maturation phases (Figure 4A). Gene expression patterns in the cultured hiPSCs are shown in Figure 4B. *NANOG* was downregulated during induction. *T* and *MIXL1* were transiently upregulated on day 5. *RUNX2* and *SP7* were also upregulated on day 5; their expression levels were maintained and statistically significant on day 23 compared with day 0. *IBSP* and *COL1A1* were significantly upregulated on days 19 and 23, respectively. The contribution of Hh signaling to osteoblast-related gene expression might cause differences in the gene expression pattern between human and mouse cells, as previously reported by Plaisant et al. (2009). On day 23, RUNX2 protein was evenly expressed in cell clusters, and SP7 was expressed in the periphery, where RUNX2 and SP7 were colocalized (Figure 4C). Calcification on days 19 and 23 was significantly higher than that on day 5 (Figures 4D and 4E). These results suggest that the present strategy is capable of differentiating hiPSCs into osteoblasts.

This study demonstrates the robust generation of osteoblasts from pluripotent stem cells using four small molecules under serum-free and feeder-free conditions. This strategy requires no or very little use of confounding factors derived from serum and feeder cells. Such a simple, small molecule-based system offers significant benefits for skeletal research and regenerative medicine by minimizing costs and maintaining the stability of the inducers. However, this study has two major limitations. First, the target molecules of TH are unclear; we are currently screening for these targets using a proteomic approach with a modified TH carrying a moiety that binds to magnetic beads via an amide bond. Second, we used Matrigel, which was not a fully defined reagent (Hughes et al., 2010), for hiPSCs to maintain cell viability. Because we observed a substantial level of hiPSC death on the Matrigel-coated plates during the initial 5-day induction, this strategy might be deleterious for the survival and differentiation of hiPSCs. In future studies, there will be a need for defined reagents suppressing the cell death of hiPSCs as well as reagents that will eliminate residual pluripotent cells (Ben-David and Benvenisty, 2011; Tang et al., 2011); the 2.3 kb Col1a1-GFP may be used to sort out osteoblasts. In conclusion, the present stepwise differentiation strategy offers a tool for in vitro mechanistic studies of osteoblast development and stem cell-based therapies for massive bone defects, although the strategy will need to be further optimized to enable broader application.

EXPERIMENTAL PROCEDURES

Differentiation of mESCs into Osteoblasts

mESCs were seeded at 100,000 cells/cm^2 in gelatin-coated 6-well plates and cultured for 24 hr in 2i culture media (see Supplemental Experimental Procedures) supplemented with CHIR (Wako Pure Chemical Industries, 039-20831; Axon Medchem, 1386), PD0325901 (Wako; 163-24001), and LIF (Millipore; ESG1107). After briefly washing the cells with PBS, the 5-day induction protocol was initiated to differentiate the cells toward a mesoderm lineage. 2i culture media without CHIR, PD0325901, or LIF were used as basal media during the differentiation culture and supplemented with small molecules for each differentiation step as shown below. The mesoderm induction was achieved by culturing the cells with 30 μM CHIR and 5 μM Cyc (Enzo Life Sciences; BML-GR334) in 2i culture media. To induce osteoblast differentiation, we then cultured the cells for 14 days in 2i culture media supplemented with 50 μg/ml ascorbic acid phosphate (AsAP) (Sigma-Aldrich; A4034), 10 mM β-glycerophosphate (β-GP) (Sigma-Aldrich; G9422), 0.1 μM dexamethasone (Dex) (Wako; 041-18861), 1 μM SAG (Calbiochem; 566660), and 1 μM TH (synthesized by Takeda Chemical Industries). For osteoblast maturation, the cells were cultured for an additional 4 days in 2i

Figure 4. Differentiation of hiPSCs into Osteoblasts

(A) A schematic showing the strategy for inducing osteoblast differentiation of hiPSCs. The lower panels show the morphology of colonies of hiPSCs and induced cells on days 0, 5, 19, and 23. Scale bars, 100 μm.

(B) Expressions of pluripotency-related (*NANOG*), mesoderm-related (*T* and *MIXL1*), and osteoblast-related genes (*RUNX2*, *SP7*, *COL1A1*, and *IBSP*) on days 0 (white bars), 5 (gray bars), 19, and 23 (black bars) in hiPSCs. The data are expressed as the mean ± SEM from six independent experiments. *$p < 0.05$ versus day 0; **$p < 0.01$ versus day 0.

(C) Protein expressions of RUNX2 and SP7 in hiPSCs on day 23. Lower panels show magnified views of the region marked by a dotted rectangular box in the left-upper panel. Nuclei are shown in pseudocolor. The arrow shows the surface of the cell cluster. Scale bars, 100 μm.

(D) Alizarin red staining on days 5, 19, and 23 in hiPSCs cultured according to the present strategy.

(E) Alizarin red staining-based quantification of calcification in hiPSCs cultured according to the present strategy, relative to that of day 5. **$p < 0.01$ versus day 5. The data are expressed as the mean ± SEM from six independent experiments.

culture media supplemented with AsAP, β-GP, and Dex. The culture media were replaced daily. TH can be distributed upon request.

SUPPLEMENTAL INFORMATION

Supplemental Information includes Supplemental Experimental Procedures, three figures, and two tables and can be found with this article online at http://dx.doi.org/10.1016/j.stemcr.2014.04.016.

ACKNOWLEDGMENTS

We thank Dr. M.J. Owen for his kind gift of the *Runx2* knockout ESCs and Dr. Andrew P. McMahon for his helpful input. This work was supported by Grants-in-Aid for Scientific Research (#23689079), the Center for Medical System Innovation, the Graduate Program for Leaders in Life Innovation, Core-to-Core Program A (Advanced Research Networks), the Funding Program for World-Leading Innovative R&D on Science and Technology, the Center for NanoBio Integration, the S-innovation program, Nakayama Foundation for Human Science and the Nakatomi Foundation Research Grant.

Received: July 9, 2013
Revised: April 24, 2014
Accepted: April 28, 2014
Published: May 22, 2014

REFERENCES

Akiyama, H., Kim, J.E., Nakashima, K., Balmes, G., Iwai, N., Deng, J.M., Zhang, Z., Martin, J.F., Behringer, R.R., Nakamura, T., and de Crombrugghe, B. (2005). Osteo-chondroprogenitor cells are derived from Sox9 expressing precursors. Proc. Natl. Acad. Sci. USA *102*, 14665–14670.

Bain, J., Plater, L., Elliott, M., Shpiro, N., Hastie, C.J., McLauchlan, H., Klevernic, I., Arthur, J.S.C., Alessi, D.R., and Cohen, P. (2007). The selectivity of protein kinase inhibitors: a further update. Biochem. J. *408*, 297–315.

Ben-David, U., and Benvenisty, N. (2011). The tumorigenicity of human embryonic and induced pluripotent stem cells. Nat. Rev. Cancer *11*, 268–277.

Bilousova, G., Jun, H., King, K.B., De Langhe, S., Chick, W.S., Torchia, E.C., Chow, K.S., Klemm, D.J., Roop, D.R., and Majka, S.M. (2011). Osteoblasts derived from induced pluripotent stem cells form calcified structures in scaffolds both in vitro and in vivo. Stem Cells *29*, 206–216.

Buttery, L.D.K., Bourne, S., Xynos, J.D., Wood, H., Hughes, F.J., Hughes, S.P.F., Episkopou, V., and Polak, J.M. (2001). Differentiation of osteoblasts and in vitro bone formation from murine embryonic stem cells. Tissue Eng. *7*, 89–99.

Davis, L.A., and Zur Nieden, N.I. (2008). Mesodermal fate decisions of a stem cell: the Wnt switch. Cell. Mol. Life Sci. *65*, 2658–2674.

Hojo, H., Ohba, S., Yano, F., Saito, T., Ikeda, T., Nakajima, K., Komiyama, Y., Nakagata, N., Suzuki, K., Takato, T., et al. (2012). Gli1 protein participates in Hedgehog-mediated specification of osteoblast lineage during endochondral ossification. J. Biol. Chem. *287*, 17860–17869.

Hojo, H., Ohba, S., Taniguchi, K., Shirai, M., Yano, F., Saito, T., Ikeda, T., Nakajima, K., Komiyama, Y., Nakagata, N., et al. (2013). Hedgehog-Gli activators direct osteo-chondrogenic function of bone morphogenetic protein toward osteogenesis in the perichondrium. J. Biol. Chem. *288*, 9924–9932.

Hughes, C.S., Postovit, L.M., and Lajoie, G.A. (2010). Matrigel: a complex protein mixture required for optimal growth of cell culture. Proteomics *10*, 1886–1890.

Jaiswal, N., Haynesworth, S.E., Caplan, A.I., and Bruder, S.P. (1997). Osteogenic differentiation of purified, culture-expanded human mesenchymal stem cells in vitro. J. Cell. Biochem. *64*, 295–312.

Kao, C.L., Tai, L.K., Chiou, S.H., Chen, Y.J., Lee, K.H., Chou, S.J., Chang, Y.L., Chang, C.M., Chen, S.J., Ku, H.H., and Li, H.Y. (2010). Resveratrol promotes osteogenic differentiation and protects against dexamethasone damage in murine induced pluripotent stem cells. Stem Cells Dev. *19*, 247–258.

Kawaguchi, J., Mee, P.J., and Smith, A.G. (2005). Osteogenic and chondrogenic differentiation of embryonic stem cells in response to specific growth factors. Bone *36*, 758–769.

Komori, T., Yagi, H., Nomura, S., Yamaguchi, A., Sasaki, K., Deguchi, K., Shimizu, Y., Bronson, R.T., Gao, Y.H., Inada, M., et al. (1997). Targeted disruption of Cbfa1 results in a complete lack of bone formation owing to maturational arrest of osteoblasts. Cell *89*, 755–764.

Levi, B., Hyun, J.S., Montoro, D.T., Lo, D.D., Chan, C.K., Hu, S., Sun, N., Lee, M., Grova, M., Connolly, A.J., et al. (2012). In vivo directed differentiation of pluripotent stem cells for skeletal regeneration. Proc. Natl. Acad. Sci. USA *109*, 20379–20384.

Li, F., Bronson, S., and Niyibizi, C. (2010). Derivation of murine induced pluripotent stem cells (iPS) and assessment of their differentiation toward osteogenic lineage. J. Cell. Biochem. *109*, 643–652.

Long, F.X., Chung, U.I., Ohba, S., McMahon, J., Kronenberg, H.M., and McMahon, A.P. (2004). Ihh signaling is directly required for the osteoblast lineage in the endochondral skeleton. Development *131*, 1309–1318.

Maeda, Y., Hojo, H., Shimohata, N., Choi, S., Yamamoto, K., Takato, T., Chung, U.I., and Ohba, S. (2013). Bone healing by sterilizable calcium phosphate tetrapods eluting osteogenic molecules. Biomaterials *34*, 5530–5537.

Marks, H., Kalkan, T., Menafra, R., Denissov, S., Jones, K., Hofemeister, H., Nichols, J., Kranz, A., Stewart, A.F., Smith, A., and Stunnenberg, H.G. (2012). The transcriptional and epigenomic foundations of ground state pluripotency. Cell *149*, 590–604.

Martí, E., and Bovolenta, P. (2002). Sonic hedgehog in CNS development: one signal, multiple outputs. Trends Neurosci. *25*, 89–96.

Nizzardo, M., Simone, C., Falcone, M., Locatelli, F., Riboldi, G., Comi, G.P., and Corti, S. (2010). Human motor neuron generation from embryonic stem cells and induced pluripotent stem cells. Cell. Mol. Life Sci. *67*, 3837–3847.

Ohba, S., Ikeda, T., Kugimiya, F., Yano, F., Lichtler, A.C., Nakamura, K., Takato, T., Kawaguchi, H., and Chung, U.I. (2007a). Identification of a potent combination of osteogenic genes for bone regeneration using embryonic stem (ES) cell-based sensor. FASEB J. *21*, 1777–1787.

Ohba, S., Nakajima, K., Komiyama, Y., Kugimiya, F., Igawa, K., Itaka, K., Moro, T., Nakamura, K., Kawaguchi, H., Takato, T., and Chung, U.I. (2007b). A novel osteogenic helioxanthin-derivative acts in a BMP-dependent manner. Biochem. Biophys. Res. Commun. *357*, 854–860.

Okabe, M., Ikawa, M., Kominami, K., Nakanishi, T., and Nishimune, Y. (1997). 'Green mice' as a source of ubiquitous green cells. FEBS Lett. *407*, 313–319.

Phillips, B.W., Belmonte, N., Vernochet, C., Ailhaud, G., and Dani, C. (2001). Compactin enhances osteogenesis in murine embryonic stem cells. Biochem. Biophys. Res. Commun. *284*, 478–484.

Plaisant, M., Fontaine, C., Cousin, W., Rochet, N., Dani, C., and Peraldi, P. (2009). Activation of hedgehog signaling inhibits osteoblast differentiation of human mesenchymal stem cells. Stem Cells *27*, 703–713.

Rodda, S.J., and McMahon, A.P. (2006). Distinct roles for Hedgehog and canonical Wnt signaling in specification, differentiation and maintenance of osteoblast progenitors. Development *133*, 3231–3244.

St-Jacques, B., Hammerschmidt, M., and McMahon, A.P. (1999). Indian hedgehog signaling regulates proliferation and differentiation of chondrocytes and is essential for bone formation. Genes Dev. *13*, 2072–2086.

Tai, G.P., Polak, J.M., Bishop, A.E., Christodoulou, I., and Buttery, L.D.K. (2004). Differentiation of osteoblasts from murine embryonic stem cells by overexpression of the transcriptional factor osterix. Tissue Eng. *10*, 1456–1466.

Tang, C., Lee, A.S., Volkmer, J.P., Sahoo, D., Nag, D., Mosley, A.R., Inlay, M.A., Ardehali, R., Chavez, S.L., Pera, R.R., et al. (2011). An antibody against SSEA-5 glycan on human pluripotent stem cells enables removal of teratoma-forming cells. Nat. Biotechnol. *29*, 829–834.

Tu, X., Joeng, K.S., and Long, F. (2012). Indian hedgehog requires additional effectors besides Runx2 to induce osteoblast differentiation. Dev. Biol. *362*, 76–82.

Wang, Y., Zhou, Z., Walsh, C.T., and McMahon, A.P. (2009). Selective translocation of intracellular Smoothened to the primary cilium in response to Hedgehog pathway modulation. Proc. Natl. Acad. Sci. USA *106*, 2623–2628.

Ye, J.H., Xu, Y.J., Gao, J., Yan, S.G., Zhao, J., Tu, Q., Zhang, J., Duan, X.J., Sommer, C.A., Mostoslavsky, G., et al. (2011). Critical-size calvarial bone defects healing in a mouse model with silk scaffolds and SATB2-modified iPSCs. Biomaterials *32*, 5065–5076.

Ying, Q.L., Wray, J., Nichols, J., Batlle-Morera, L., Doble, B., Woodgett, J., Cohen, P., and Smith, A. (2008). The ground state of embryonic stem cell self-renewal. Nature *453*, 519–523.

Zhang, X., Peterson, K.A., Liu, X.S., McMahon, A.P., and Ohba, S. (2013). Gene regulatory networks mediating canonical Wnt signal-directed control of pluripotency and differentiation in embryo stem cells. Stem Cells *31*, 2667–2679.

zur Nieden, N.I., Kempka, G., and Ahr, H.J. (2003). In vitro differentiation of embryonic stem cells into mineralized osteoblasts. Differentiation *71*, 18–27.

Biomedical Research (Tokyo) 35 (4) 263-270, 2014

Determination of differential gene expression profiles in superficial and deeper zones of mature rat articular cartilage using RNA sequencing of laser microdissected tissue specimens

Yoshifumi MORI[1], Ung-il CHUNG[2], Sakae TANAKA[1], and Taku SAITO[1, 3]

[1] Sensory & Motor System Medicine, [2] Center for Disease Biology and Integrative Medicine, Faculty of Medicine, [3] Bone and Cartilage Regenerative Medicine, University of Tokyo, 7-3-1 Hongo, Bunkyo-ku, Tokyo 113-8655, Japan

(Received 16 May 2014; and accepted 27 May 2014)

ABSTRACT

Superficial zone (SFZ) cells, which are morphologically and functionally distinct from chondrocytes in deeper zones, play important roles in the maintenance of articular cartilage. Here, we established an easy and reliable method for performance of laser microdissection (LMD) on cryosections of mature rat articular cartilage using an adhesive membrane. We further examined gene expression profiles in the SFZ and the deeper zones of articular cartilage by performing RNA sequencing (RNA-seq). We validated sample collection methods, RNA amplification and the RNA-seq data using real-time RT-PCR. The combined data provide comprehensive information regarding genes specifically expressed in the SFZ or deeper zones, as well as a useful protocol for expression analysis of microsamples of hard tissues.

Osteoarthritis (OA), a chronic degenerative joint disorder characterized by articular cartilage destruction, is a major public health issue, causing pain and disability of the elderly worldwide (5, 8). Although effective disease-modifying treatments for OA have not been developed, its etiopathogenesis has been addressed in recent clinical studies. Cartilage degeneration is first observed at the articular surface in the form of fibrillation (24). Once the surface is disrupted, deeper cartilage layers are subsequently degraded (24).

Articular cartilage (AC) is composed of three layers: the superficial (SFZ), middle and deep zones. The SFZ, the outermost surface layer adjacent to the joint cavity, is histologically distinct from the deeper zones. In the SFZ, collagen fibers align parallel to the articular surface, in contrast to their vertical alignment in the deeper layers (2, 17). SFZ cells, which also display parallel alignment, are smaller than chondrocytes in the deeper layers and exhibit characteristic flat morphology (10). SFZ cells produce lubricin, encoded by *Proteoglycan4* (*Prg4*), for surface lubrication. An homozygous mutant of the human *PRG4* gene causes the autosomal recessive camptodactyly-arthropathy-coxa vara-pericarditis syndrome that shows congenital or early-onset camptodactyly and childhood-onset noninflammatory arthropathy (1, 16). Mice lacking *Prg4* (*Prg4*$^{-/-}$) exhibit early onset of osteoarthritis (25). In addition, chondrocytes obtained from SFZ display higher proliferative activity than those from deeper AC zones, implying that SFZ might be the main cell source of cartilage regeneration (32). Despite the potential roles of SFZ in the etiopathogenesis and pathophysiology of OA, apart from the involvement of Wnt/β-catenin signaling, TGF-β/BMP signaling and high mobility group box 2 (HMGB2), molecular mechanisms regulating the differentiation and maintenance of SFZ are still unknown (12, 22, 28). This lack of data is mainly because comprehensive *in vivo* gene expression analysis of the SFZ is difficult due to its thinness, which makes it difficult to obtain SFZ-spe-

Address correspondence to: Taku Saito, M.D., Ph.D., Associate Professor
Bone and Cartilage Regenerative Medicine, Faculty of Medicine, University of Tokyo, Hongo 7-3-1, Bunkyo-ku, Tokyo 113-8655, Japan
Tel: +81-3-3815-5411 (ext. 37369), Fax: +81-3-3818-4082
E-mail: tasaitou-tky@umin.ac.jp

cific samples.

To address this issue, we focused on a microsampling technique based on laser microdissection (LMD). LMD is an innovative technology that enables the isolation of a micro-area of tissue and has been widely used for a variety of biological research. Although LMD from a frozen sample is the ideal method for collection of RNA, preparation of a cryosection from hard tissue is difficult by conventional methods. In the present study, we aimed to establish an easy and reliable method for performance of LMD on cryosections of mature rat articular cartilage and for subsequent performance of RNA sequencing (RNA-seq) to obtain gene expression profiles for both the SFZ and deeper AC zones.

MATERIALS AND METHODS

Specimen preparation. All animal experiments were undertaken according to the guidelines of the Animal Care and Use Committee of the University of Tokyo. Ten-week-old male Sprague Dawley rats (Sankyo Laboratories, Tokyo, Japan) were sacrificed by cervical dislocation under anesthesia. A ring-shaped skin incision was made at the height of the rib cage, the skin was dragged distally and the distal flap was inverted to expose the lower extremities. The left knee was then disarticulated, the medial and lateral menisci were detached and the tibia was cut at its shaft. The proximal tibia was immediately and directly placed into liquid nitrogen. Frozen sections were embedded in pre-cooled SCEM compound (Section-lab, Hiroshima, Japan) and stored at −80°C until further analysis.

For H&E staining, 10-μm paraffin-embedded sections were prepared from 10-week-old Sprague Dawley rats as described previously (18). H&E staining was performed according to a standard protocol.

Laser microdissection (LMD). We performed LMD using frozen sections prepared by Kawamoto's film method (11, 20). Specimens were placed into a Leica CM3050S (Leica Microsystems, Wetzlar, Germany) at −30°C and cut coarsely in a frontal plane until a desired surface was exposed. The adhesive surface of Cryofilm Type IIC (Section-lab) was then attached to the specimen and 10-μm-thick sections were cut. The specimen with attached film was fixed to a metal frame using a double-sided tape (Nichiban, Tokyo, Japan). This metal frame was prepared from a membrane slide (PEN-membrane, 2.0 μm) whose PEN-membrane was removed prior to use. The fixed specimen and attached film were stored in the gas layer of liquid nitrogen until microdissection.

To prevent RNA degradation, frozen specimens (prior to thawing) were immediately soaked in 80% ethanol for 30 s, then in 100% ethanol for 1 min (twice), then in xylene for 5 min at room temperature and subsequently they were dried for 5 min. Specimens were then placed in a Leica LMD6500 (Leica Microsystems). Microdissection of the section was performed using the following settings: Power 50, Aperture 30 and Speed 5. Samples were collected in the cap of a 200 μL tube pre-filled with 50 μL of XB buffer of the Arcturus Picopure RNA isolation Kit (Thermo Fisher Scientific, Waltham, MA). SFZ and deeper AC samples from two slices were obtained for each rat. Samples were stored at −80 °C until mRNA extraction.

RNA extraction and amplification. RNA extraction was performed using the Picopure RNA isolation Kit according to the manufacturer's protocol. RNA was collected in 11 μL of EB buffer, 1.5 μL of which were then used for checking RNA purity using NanoDrop (Thermo Fisher Scientific). We then amplified the remaining sample by two rounds of *in-vitro* transcription using the Arcturus RiboAmp HS PLUS kit (Thermo Fisher Scientific) according to the manufacturer's protocol. Amplified RNA (aRNA) was obtained in 30 μL of RNA elution buffer, 1.5 μL of which were again analyzed using NanoDrop to check quantity and purity.

Real-time RT-PCR. One microgram of aRNA was reverse-transcribed using the QuantiTect Reverse-Transcription kit (Qiagen, Hilden, Germany) without performing the genomic DNA elimination reaction. The resultant 20 μL of cDNA solution was diluted to 100 μL with distilled water. For real-time RT-PCR analysis, the quantity of DNA polymerase was increased versus the standard protocol to rapidly amplify aRNAs with a small copy number (4). Reagents were prepared as follows: FastStart Universal SYBR Green Master (Roche Diagnostics, Basel, Switzerland) 10 μL; FastStart Taq DNA Polymerase (5 U/μL, Roche) 0.4 μL; forward Primer (10 μM) 2 μL; Reverse Primer (10 μM) 2 μL; distilled water 3.6 μL, aRNA solution 2 μL, and were run in triplicate on a Thermal Cycler Dice (Takara Bio, Otsu, Japan). Relative expression levels were calculated by the delta-delta CT method using *Gapdh* as an internal control. Primer pairs used are shown in Table 1.

RNA sequencing (RNA-seq). A cDNA library was constructed according to the TrueSeq RNA Sample

Table 1 *List of primers used for real-time RT-PCR*

Gene	Forward primer	Reverse primer	Product size (bp)
Gapdh	TGCACCACCAACTGCTTAGC	GGATGCAGGGATGATGTTCT	177
Col2a1	ATGACTTTCCTCCGTCTACTGTCC	TGATGGTCTTGCCCCACTTAC	226
Prg4	AACCTGACTGGCAAAGAAGAATG	TGGGAGGAAGAGGAGGAATAAATAG	232
Bmp7	GCCCTTCCTTTCCGTTCTATTT	CATCCCTCACCGACCTCTTC	129
Tmem176a	CGTCAGGCAGGAAGAAGACC	GGTGGTGAAGGCAGAGGAGA	117
Wnt9a	TGGCAGTGGACACACAAGG	TCGCCACACAGTTGAGGTAGA	80
Frzb	GGGAACTCATGGTGCCTTTT	GGAATGAGACTTTTAGGTGATTGG	80
Ibsp	CAAACATGAATACACGGTGTGAG	TTATCTGTAGGGGAGGGGTTGT	93
Grem1	GATTATGCAGGCTATGACGGAAC	GCCAAATTAGCTTCTATGAGACCA	85

Preparation V2 Guide Rev. C (Illumina, San Diego, CA) and sequencing was performed using HiSeq 2000 (Illumina) according to the manufacturer's protocol. Then we normalized the sequence data by trimmed mean of M values method (26). The raw and processed data are available on GEO database with accession number GSE57377. After changing the measured value less than one to one, we calculated the fold change between SFZ and deeper AC.

Statistical analysis. Differences in mRNA expression levels between the SFZ and deeper AC as measured by real-time RT-PCR were analyzed using a paired *t*-test.

RESULTS

Histological evaluation of articular cartilage

In H&E-stained paraffin sections of the proximal tibia, the SFZ was easily distinguishable from deeper AC layers by its flat-shaped nuclei and its alignment parallel to the joint surface (Fig. 1A, left). The SFZ was also easily distinguishable without any staining in frozen sections on adhesive membrane (Fig. 1A, right). We therefore performed LMD on unstained sections.

LMD, RNA purification and amplification

Both SFZ and deeper AC layers were easily cut and collected using LMD. We obtained a pair of SFZ and deeper AC samples from each of seven rats. After purification using the Picopure RNA isolation kit and amplification using the RiboAmp HS Plus kit, we ultimately obtained 4.1 to 28.0 μg aRNA from SFZ samples, and 4.0 to 74.6 μg from deeper AC samples.

Validation of accurate sampling by real-time RT-PCR

After reverse-transcription of one μg aRNA, the accuracy of our sampling was validated by real-time RT-PCR. Previous studies showed that *Prg4* is upregulated and *Col2a1* is downregulated in the SFZ compared to deeper AC (3, 21, 23, 25). Our real-time RT-PCR results showed significant upregulation of *Prg4* and downregulation of *Col2a1* in SFZ as compared to deeper AC, indicating that our differential sampling from these two distinct areas was appropriate (Fig. 1B).

RNA-seq

RNA-seq was performed on two pairs of SFZ and deeper AC samples. Fold change in expression of a gene between SFZ and deeper AC was averaged for two pairs (rat 1 and rat 2), and genes with more than a 2-fold change (log2) on average were selected for further study. In total, 133 genes were found to be upregulated in SFZ and 758 genes were upregulated in deeper AC. The top 20 upregulated genes in SFZ and deeper AC are listed in Tables 2 and 3, respectively. Genes displaying lower fold changes are listed in Supplementary Tables S1 and S2, respectively. The present data showed upregulation of SFZ marker genes including *Wnt9a*, *Col1a1*, *Errfi1*, *Clu*, *Thbs4*, *Igfbp5* and *Prg4* in the SFZ (9, 15, 21, 25, 27, 32), confirming that we appropriately collected RNA samples from SFZ and deeper AC.

Validation of RNA-seq results by real-time RT-PCR

To confirm the reproducibility of the expression patterns obtained by RNA-seq, we analyzed the expression patterns of the three genes that displayed the highest fold change in the SFZ compared to deeper AC (*Bmp7*, *Tmem176a*, and *Wnt9a*) and those in deeper AC compared to the SFZ (*Frzb*, *Ibsp* and *Grem1*) using real-time RT-PCR. The expression

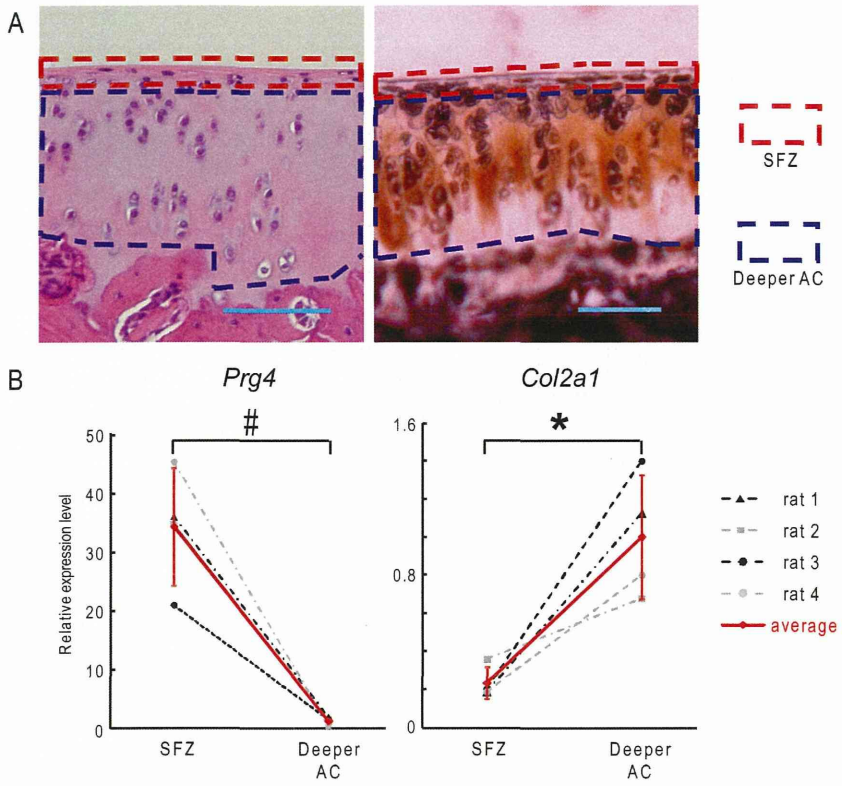

Fig. 1 Microscopic and real-time RT-PCR analysis of articular cartilage zones and chondrocytes. (**A**) H&E staining of a paraffin-embedded section (left panel) and a frozen section on an adhesive membrane (right panel) of adult rat proximal tibia. Red and blue dashed line boxes indicate the superficial zone (SFZ) and deeper articular cartilage (AC), respectively. Scale bars, 100 μm. (**B**) mRNA levels of *Prg4* and *Col2a1* in chondrocytes in the SFZ and deeper AC from four rats (rat 1 to 4), determined using real-time RT-PCR. All data are shown as means ± SD. $^{*}P < 0.05$, $^{\#}P < 0.005$.

patterns of all six genes as determined by real-time RT-PCR were similar to those determined by RNA-seq (Fig. 2). Significant differences were observed in the mRNA levels of all genes except for *Bmp7* between the two zones, consistent with the results of the RNA-seq (Fig. 2).

DISCUSSION

In the present study, we analyzed gene expression profiles of chondrocytes in the SFZ and deeper zones of mature rat articular cartilage using RNA-seq of laser microdissected tissue specimens. Since the articular cartilage is adjacent to the subchondral bone and the SFZ is extremely narrow, we had to optimize the conditions for all steps of protocol including preparation of a fine cryosection from hard tissue, specific dissection of SFZ, and reliable amplification of a small amount of RNA. Here, we established for the first time a successful procedure for examination of the RNA expression profile of a micro-region of hard tissue using a combination of cryosectioning employing an adhesive membrane, LMD and RNA-seq.

Recent studies indicate that SFZ cells play essential roles in the homeostasis of articular cartilage (25, 27, 28, 32). The previous studies analyzed the expression of genes in SFZ by performing microarray analysis of SFZ cells isolated from neonatal mouse knee joints by digestion with trypsin and collagenase. However, the enzymatic treatment procedure might change the gene expression profile of SFZ from that *in vivo* (32). Since LMD is now the most commonly used commercially available microsampling procedure, we decided to use LMD for specific collection of SFZ cells. Although LMD has been widely used for sampling RNA, its application to a hard tissue such as bone has been rarely reported because of the difficulty of preparing fine cryosections of such tissue. Some previous studies reported LMD sampling of soft immature cartilage of rodent embryos or infants (31, 33). However, in our pre-

Table 2 *List of top 20 genes with higher expression in the SFZ than in deeper AC*

Gene Symbol	Description	Fold Change (log2)
Bmp7	bone morphogenetic protein 7	51.5
Tmem176a	transmembrane protein 176A	45.3
Wnt9a	wingless-type MMTV integration site family, member 9A	32.7
Gldc	glycine dehydrogenase (decarboxylating)	26.5
Mov10	Moloney leukemia virus 10	24.5
Prss23	protease, serine, 23	23.6
Cidea	cell death-inducing DFFA-like effector a	23.4
Cdh13	cadherin 13	23.3
Col1a1	collagen, type I, alpha 1	22.7
Kcnj8	potassium inwardly-rectifying channel, subfamily J, member 8	20.7
Slc8a1	solute carrier family 8 (sodium/calcium exchanger), member 1	19.6
Lrrc52	leucine rich repeat containing 52	19.6
Bend5	BEN domain containing 5	18.8
Sass6	spindle assembly 6 homolog (*C. elegans*)	18.4
Kera	keratocan	16.5
Dact2	dapper, antagonist of beta-catenin, homolog 2 (*Xenopus laevis*)	16.5
Cldn11	claudin 11	16.3
Pion	pigeon homolog (Drosophila)	13.6
Htra4	HtrA serine peptidase 4	13.3
Arsi	arylsulfatase family, member I	13.1

Table 3 *List of top 20 genes with higher expression in deeper AC than in the SFZ*

Gene Symbol	Description	Fold Change (log2)
Frzb	frizzled-related protein	55.8
Ibsp	integrin-binding sialoprotein	45.9
Grem1	gremlin 1	45.5
Rarres1	retinoic acid receptor responder (tazarotene induced) 1	43.9
Dmp1	dentin matrix acidic phosphoprotein 1	40.9
Tnni2	troponin I type 2 (skeletal, fast)	38.7
Gfap	glial fibrillary acidic protein	35.0
Arhgap18	Rho GTPase activating protein 18	33.7
F5	coagulation factor V (proaccelerin, labile factor)	32.8
Etnk2	ethanolamine kinase 2	31.9
Ogfrl1	opioid growth factor receptor-like 1	31.4
R3hdml	R3H domain (binds single-stranded nucleic acids) containing-like	28.6
Mns1	meiosis-specific nuclear structural 1	27.4
Evi2a	ecotropic viral integration site 2A	26.3
Phospho1	phosphatase, orphan 1	26.0
Steap4	STEAP family member 4	25.8
Sptlc3	serine palmitoyltransferase, long chain base subunit 3	23.8
A2m	alpha-2-macroglobulin	23.6
Irx4	iroquois homeobox 4	23.6
Il17b	interleukin 17B	23.2

liminary experiment, we were unable to make fine cryosections using the conventional methods due to subchondral bone beneath the articular cartilage. To overcome the difficulty, we adapted an unique cryosection method that uses an adhesive membrane to support the fine structure of the original tissue during the slicing procedure (11, 20). In addition to using the method, we also immediately dehydrated the sliced sections to facilitate the subsequent LMD. Using the modified cryosection method we efficiently obtained RNA from micro-areas of the fine cryosections.

Since only a small amount of RNA can be obtained using the LMD method, an amplification pro-

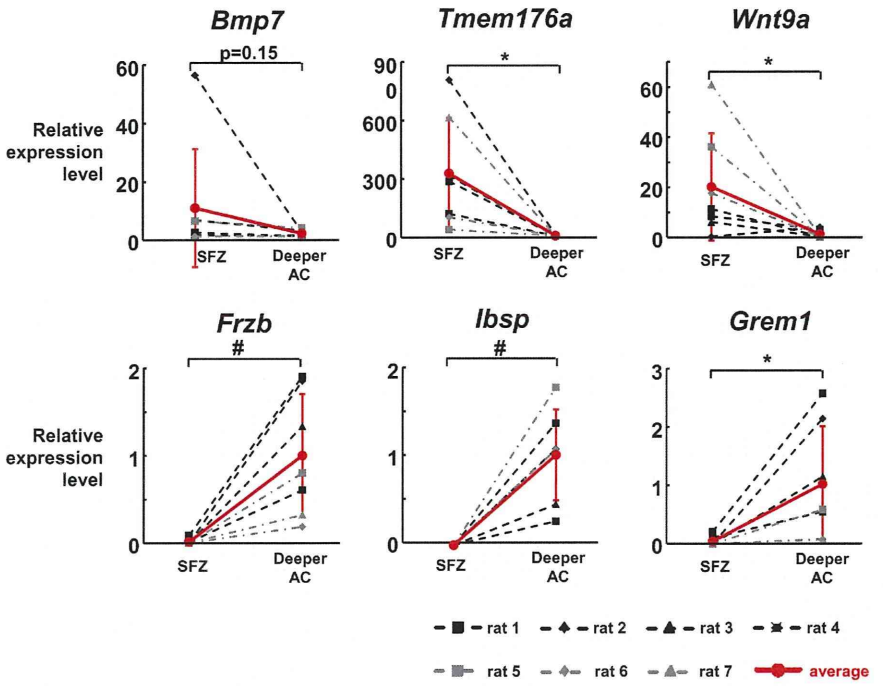

Fig. 2 mRNA levels of the three genes with the highest fold change in the SFZ compared to deeper AC (*Bmp7*, *Tmem176a*, and *Wnt9a*) and those in deeper AC compared to the SFZ (*Frzb*, *Ibsp*, and *Grem1*), in cartilage of SFZ and deeper AC from seven rats (rat 1 to 7) determined by real-time RT-PCR. All data are shown as means ± SD. $^{*}P < 0.05$, $^{\#}P < 0.005$.

cedure is indispensable for further gene expression analysis. Of several commercial amplification kits that we tested, the RiboAmp HS Plus kit provided the most reproducible results in quantification of representative marker genes by real-time RT-PCR. However, because this amplification system utilizes an *in vitro* transcription method, it can only amplify mRNA but not microRNA. Combination of our method with other novel methods should make it possible to further analyze other types of RNA or DNA in the future.

Microarray technology has been a standard method for comprehensive gene expression analysis for many years. Numerous data have been accumulated in previous studies using microarray analyses. However, microarray analysis has several limitations, including background noise, that arise from hybridization of cDNA samples and probes and also has an upper limit of signal strength (19, 30). On the other hand, gene quantification using RNA-seq is based on the number of sequences read, therefore upper or lower limits of signal strength do not exist. In addition, RNA-seq is free from mishybridization, a major cause of false positive signals in microarray analysis (19, 30).

In addition to previously reported marker genes of the SFZ or deeper AC, the present data revealed distinct zone expression of several important molecules. Of the genes that were upregulated in the SFZ, *Bmp7* showed the highest fold change (Table 2), although significant difference was not observed in the mRNA levels of *Bmp7* between the two zones due to the high variability in its expression level in the SFZ (Fig. 2). Bmp7 stimulates *Prg4* expression in articular cartilage explants and cultured articular chondrocytes (12, 22). Based on these results, Bmp7 may function to stimulate production of ECM components in SFZ in a paracrine fashion. Of the genes that were upregulated in deeper AC, Wnt signaling antagonists including *Frzb*, *Grem1* and *Dkk1* were highly upregulated with an average fold change value of 55.77, 45.52 and 4.01, respectively (Table 3, Supplementary Table S2). Leijten *et al.* reported that these three genes are upregulated in articular cartilage compared to growth plate cartilage based on microarray analysis of samples from adolescent human donors (14). In long-bone explant organ culture and in human mesenchymal stem cell culture, treatment with these proteins suppressed hypertrophic differentiation without affecting chondrogenesis (14), indicating that these genes may direct immature chondrocytes to mature articular chondrocytes, not

to growth plate chondrocytes. Combined with our findings, the three genes may keep the character of articular chondrocytes in deeper zones from that of the SFZ cells or growth plate chondrocytes. Furthermore, Wnt/β-catenin signaling is activated in the SFZ and stimulates SFZ-cell proliferation and Prg4 production (13, 32). All of these findings support the idea that distinct regulation of Wnt/β-catenin signaling is essential for maintenance of the SFZ and deeper AC.

Fukui *et al.* previously performed microarray analysis of LMD samples obtained from the knee joint cartilage of OA patients (6, 7). They found that the gene expression patterns of chondrocytes differed according to the layer of articular cartilage in which they were situated, indicating that different phenotypes of articular chondrocytes in each layer may be essential for homeostasis of articular cartilage (6). In particular, the SFZ is indubitably the most potent layer for maintenance and repair of articular joints (25, 27, 28). Furthermore, studies of the rodent OA model have demonstrated many molecules and signaling pathways that play a role in the pathophysiology of OA (29). The present data provide useful knowledge that will contribute to the development of zone-specific Cre mice and to further determination of novel molecules that regulate SFZ cells.

In conclusion, we established a reliable technique that employs cryosections with an adhesive membrane, LMD and RNA-seq for analysis of gene expression profiles of hard tissue. By using this method, we demonstrated different gene expression profiles in the SFZ and the deeper layers of rat articular cartilage. The present RNA-seq data resource will contribute to OA research aimed at further understanding the functions of SFZ.

Acknowledgments

We thank J. Sugita, R. Yamaguchi and H. Kawahara for technical assistance. This study was supported by a Grant-in-aid for Scientific Research from the Japanese Ministry of Education, Culture, Sports, Science and Technology (#24390348).

REFERENCES

1. Bahabri SA, Suwairi WM, Laxer RM, Polinkovsky A, Dalaan AA and Warman ML (1998) The camptodactyly-arthropathy-coxa vara-pericarditis syndrome: clinical features and genetic mapping to human chromosome 1. *Arthritis Rheum* **41**, 730–735.
2. Clark JM (1990) The organisation of collagen fibrils in the superficial zones of articular cartilage. *J Anat* **171**, 117–130.
3. Craig FM, Bentley G and Archer CW (1987) The spatial and temporal pattern of collagens I and II and keratan sulphate in the developing chick metatarsophalangeal joint. *Development* **99**, 383–391.
4. Erickson HS, Albert PS, Gillespie JW, Rodriguez-Canale J, Marston Linehan W, Pinto PA, Chuaqui RF and Emmert-Buck MR (2009) Quantitative RT-PCR gene expression analysis of laser microdissected tissue samples. *Nat Protoc* **4**, 902–922.
5. Felson DT and Zhang Y (1998) An update on the epidemiology of knee and hip osteoarthritis with a view to prevention. *Arthritis Rheum* **41**, 1343–1355.
6. Fukui N, Ikeda Y, Ohnuki T, Tanaka N, Hikita A, Mitomi H, Mori T, Juji T, Katsuragawa Y, Yamamoto S, Sawabe M, Yamane S, Suzuki R, Sandell LJ and Ochi T (2008) Regional differences in chondrocyte metabolism in osteoarthritis: a detailed analysis by laser capture microdissection. *Arthritis Rheum* **58**, 154–163.
7. Fukui N, Ikeda Y and Tanaka N (2011) The use of laser capture microdissection on adult human articular cartilage for gene expression analysis. *Methods Mol Biol* **755**, 449–459.
8. Guccione AA, Felson DT, Anderson JJ, Anthony JM, Zhang Y, Wilson PW, Kelly-Hayes M, Wolf PA, Kreger BE and Kannel WB (1994) The effects of specific medical conditions on the functional limitations of elders in the Framingham Study. *Am J Public Health* **84**, 351–358.
9. Hartmann C and Tabin CJ (2001) Wnt-14 plays a pivotal role in inducing synovial joint formation in the developing appendicular skeleton. *Cell* **104**, 341–351.
10. Hughes LC, Archer CW and ap Gwynn I (2005) The ultrastructure of mouse articular cartilage: collagen orientation and implications for tissue functionality. A polarised light and scanning electron microscope study and review. *Eur Cell Mater* **9**, 68–84.
11. Kawamoto T and Kawamoto K (2014) Preparation of thin frozen sections from nonfixed and undecalcified hard tissues using Kawamot's film method (2012). *Methods Mol Biol* **1130**, 149–164.
12. Khalafi A, Schmid TM, Neu C and Reddi AH (2007) Increased accumulation of superficial zone protein (SZP) in articular cartilage in response to bone morphogenetic protein-7 and growth factors. *J Orthop Res* **25**, 293–303.
13. Koyama E, Shibukawa Y, Nagayama M, Sugito H, Young B, Yuasa T, Okabe T, Ochiai T, Kamiya N, Rountree RB, Kingsley DM, Iwamoto M, Enomoto-Iwamoto M and Pacifici M (2008) A distinct cohort of progenitor cells participates in synovial joint and articular cartilage formation during mouse limb skeletogenesis. *Dev Biol* **316**, 62–73.
14. Leijten JC, Emons J, Sticht C, van Gool S, Decker E, Uitterlinden A, Rappold G, Hofman A, Rivadeneira F, Scherjon S, Wit JM, van Meurs J, van Blitterswijk CA and Karperien M (2012) Gremlin 1, frizzled-related protein, and Dkk-1 are key regulators of human articular cartilage homeostasis. *Arthritis Rheum* **64**, 3302–3312.
15. Malda J, ten Hoope W, Schuurman W, van Osch GJ, van Weeren PR and Dhert WJ (2010) Localization of the potential zonal marker clusterin in native cartilage and in tissue-engineered constructs. *Tissue Eng Part A* **16**, 897–904.
16. Marcelino J, Carpten JD, Suwairi WM, Gutierrez OM, Schwartz S, Robbins C, Sood R, Makalowska I, Baxevanis A, Johnstone B, Laxer RM, Zemel L, Kim CA, Herd JK, Ihle J, Williams C, Johnson M, Raman V, Alonso LG, Brunoni D, Gerstein A, Papadopoulos N, Bahabri SA, Trent JM and Warman ML (1999) CACP, encoding a secreted proteoglycan, is mutated in camptodactyly-arthropathy-coxa vara-peri-

carditis syndrome. *Nat Genet* **23**, 319–322.
17. Minns RJ and Steven FS (1977) The collagen fibril organization in human articular cartilage. *J Anat* **123**, 437–457.
18. Mori Y, Saito T, Chang SH, Kobayashi H, Ladel CH, Guehring H, Chung UI and Kawaguchi H (2014) Identification of fibroblast growth factor-18 as a molecule to protect adult articular cartilage by gene expression profiling. *J Biol Chem* **289**, 10192–10200.
19. Nagalakshmi U, Wang Z, Waern K, Shou C, Raha D, Gerstein M and Snyder M (2008) The transcriptional landscape of the yeast genome defined by RNA sequencing. *Science* **320**, 1344–1349.
20. Nakamura Y, Nomura Y, Arai C, Noda K, Oikawa T, Kogure K, Kawamoto T and Hanada N (2007) Laser capture microdissection of rat periodontal ligament for gene analysis. *Biotech Histochem* **82**, 295–300.
21. Nalin AM, Greenlee TK Jr. and Sandell LJ (1995) Collagen gene expression during development of avian synovial joints: transient expression of types II and XI collagen genes in the joint capsule. *Dev Dyn* **203**, 352–362.
22. Niikura T and Reddi AH (2007) Differential regulation of lubricin/superficial zone protein by transforming growth factor beta/bone morphogenetic protein superfamily members in articular chondrocytes and synoviocytes. *Arthritis Rheum* **56**, 2312–2321.
23. Pacifici M, Koyama E and Iwamoto M (2005) Mechanisms of synovial joint and articular cartilage formation: recent advances, but many lingering mysteries. *Birth Defects Res C Embryo Today* **75**, 237–248.
24. Poole AR, Guilak F and Abramson SB (2007) Etiopathogenesis of osteoarthritis. In: *Osteoarthritis.* (Moskowitz RW, Altman RD, Hochberg MC, Buckwalter JA and Goldberg VM, eds.) pp 27–49, Wolters Kluwer, Philadelphia.
25. Rhee DK, Marcelino J, Baker M, Gong Y, Smits P, Lefebvre V, Jay GD, Stewart M, Wang H, Warman ML and Carpten JD (2005) The secreted glycoprotein lubricin protects cartilage surfaces and inhibits synovial cell overgrowth. *J Clin Invest* **115**, 622–631.
26. Robinson MD and Oshlack A (2010) A scaling normalization method for differential expression analysis of RNA-seq data. *Genome Biol* **11**, R25.
27. Staal B, Williams BO, Beier F, Vande Woude GF and Zhang YW (2014) Cartilage-specific deletion of Mig-6 results in osteoarthritis-like disorder with excessive articular chondrocyte proliferation. *Proc Natl Acad Sci USA* **111**, 2590–2595.
28. Taniguchi N, Carames B, Kawakami Y, Amendt BA, Komiya S and Lotz M (2009) Chromatin protein HMGB2 regulates articular cartilage surface maintenance via beta-catenin pathway. *Proc Natl Acad Sci USA* **106**, 16817–16822.
29. Wang M, Shen J, Jin H, Im HJ, Sandy J and Chen D (2011) Recent progress in understanding molecular mechanisms of cartilage degeneration during osteoarthritis. *Ann N Y Acad Sci* **1240**, 61–69.
30. Wang Z, Gerstein M and Snyder M (2009) RNA-Seq: a revolutionary tool for transcriptomics. *Nat Rev Genet* **10**, 57–63.
31. Yamane S, Cheng E, You Z and Reddi AH (2007) Gene expression profiling of mouse articular and growth plate cartilage. *Tissue Eng* **13**, 2163–2173.
32. Yasuhara R, Ohta Y, Yuasa T, Kondo N, Hoang T, Addya S, Fortina P, Pacifici M, Iwamoto M and Enomoto-Iwamoto M (2011) Roles of beta-catenin signaling in phenotypic expression and proliferation of articular cartilage superficial zone cells. *Lab Invest* **91**, 1739–1752.
33. Zhang M, Pritchard MR, Middleton FA, Horton JA and Damron TA (2008) Microarray analysis of perichondral and reserve growth plate zones identifies differential gene expressions and signal pathways. *Bone* **43**, 511–520.

Supplementary Table S1 *List of genes with higher expression in the SFZ than in Deeper AC (ranks lower than 20th, fold change (log2) > 2)*

Gene Symbol	Description	Fold Change (log2)
Gp1bb	glycoprotein Ib (platelet), beta polypeptide	12.7
Ttll12	tubulin tyrosine ligase-like family, member 12	12.7
Aifm3	apoptosis-inducing factor, mitochondrion-associated 3	12.3
Il15	interleukin 15	10.7
Cd74	Cd74 molecule, major histocompatibility complex, class II invariant chain	10.6
Aldh1a2	aldehyde dehydrogenase 1 family, member A2	10.6
Tcp11	t-complex protein 11	10.3
Myoc	myocilin	10.0
Fbxo43	F-box protein 43	9.3
MARCH8	retinoblastoma-like 1 (p107)	9.1
Tead1	TEA domain family member 1	8.3
Rph3al	rabphilin 3A-like (without C2 domains)	8.2
Rxrg	retinoid X receptor gamma	8.2
Errfi1	ERBB receptor feedback inhibitor 1	8.0
Ntrk3	neurotrophic tyrosine kinase, receptor, type 3	7.9
Slc2a9	solute carrier family 2 (facilitated glucose transporter), member 9	7.6
Mfsd6	major facilitator superfamily domain containing 6	7.6
Nudt6	nudix (nucleoside diphosphate linked moiety X)-type motif 6	7.2
Tmprss2	transmembrane protease, serine 2	7.0
Clu	clusterin	6.5
Hs3st1	heparan sulfate (glucosamine) 3-O-sulfotransferase 1	6.5
RGD1311164	similar to DNA segment, Chr 6, Wayne State University 163, expressed	6.2
Thbs4	thrombospondin 4	6.2
Bmp4	bone morphogenetic protein 4	6.1
Arhgdib	Rho, GDP dissociation inhibitor (GDI) beta	5.5
Hbegf	heparin-binding EGF-like growth factor	5.5
Casr	calcium-sensing receptor	5.5
Mgll	monoglyceride lipase	5.3
Zc3h3	zinc finger CCCH type containing 3	5.2
Rnf208	ring finger protein 208	5.2
Prrx1	paired related homeobox 1	5.2
Adhfe1	alcohol dehydrogenase, iron containing, 1	5.1
Egfl6	EGF-like-domain, multiple 6	5.0
Igfbp5	insulin-like growth factor binding protein 5	5.0
Sema4b	Semaphorin 4B	4.9
RGD1309708	similar to RIKEN cDNA 4930455F23	4.9
Cxcl12	chemokine (C-X-C motif) ligand 12	4.7
Slc6a12	solute carrier family 6 (neurotransmitter transporter, betaine/GABA), member 12	4.6
Cdh23	cadherin 23 (otocadherin)	4.4
Ncald	neurocalcin delta	4.4

Supplementary Table S1 *(continued)*

Gene Symbol	Description	Fold Change (log2)
Itih3	inter-alpha trypsin inhibitor, heavy chain 3	4.4
Gch1	GTP cyclohydrolase 1	4.3
Pnpla2	patatin-like phospholipase domain containing 2	4.3
Scara3	scavenger receptor class A, member 3	4.1
Sectm1b	secreted and transmembrane 1B	4.1
Ifi27l2b	interferon, alpha-inducible protein 27 like 2B	4.1
Tll1	tolloid-like 1	3.9
Bik	BCL2-interacting killer (apoptosis-inducing)	3.9
Tc2n	tandem C2 domains, nuclear	3.9
Nkx6-1	NK6 homeobox 1	3.9
Scg5	secretogranin V	3.9
Lhfpl2	lipoma HMGIC fusion partner-like 2	3.9
Cdon	Cdon homolog (mouse)	3.8
Fhdc1	FH2 domain containing 1	3.7
Sult2b1	sulfotransferase family, cytosolic, 2B, member 1	3.6
Msx1	msh homeobox 1	3.6
Ampd3	adenosine monophosphate deaminase 3	3.6
Wnt11	wingless-type MMTV integration site family, member 11	3.5
Rarres2	retinoic acid receptor responder (tazarotene induced) 2	3.5
Clic2	chloride intracellular channel 2	3.5
Mfsd2a	major facilitator superfamily domain containing 2A	3.5
Gda	guanine deaminase	3.5
Plekhb1	pleckstrin homology domain containing, family B (evectins) member 1	3.3
Mgp	matrix Gla protein	3.2
Egln3	EGL nine homolog 3 (C. elegans)	3.2
Ppap2b	phosphatidic acid phosphatase type 2B	3.2
Xrcc2	X-ray repair complementing defective repair in Chinese hamster cells 2	3.1
Pigl	phosphatidylinositol glycan anchor biosynthesis, class L	3.1
Nrk	Nik related kinase	3.1
Hmcn1	hemicentin 1	3.1
MGC105649	hypothetical LOC302884	3.1
Slc40a1	solute carrier family 39 (iron-regulated transporter), member 1	3.0
Tspan13	tetraspanin 13	3.0
Optc	opticin	3.0
Sec31b	SEC31 homolog B (S. cerevisiae)	3.0
Wdfy2	WD repeat and FYVE domain containing 2	3.0
Rin2	Ras and Rab interactor 2	2.9
Dagla	diacylglycerol lipase, alpha	2.9
Jup	junction plakoglobin	2.8
Rem1	RAS (RAD and GEM)-like GTP-binding 1	2.8
Cstf3	cleavage stimulation factor, 3' pre-RNA, subunit 3	2.8
Clock	clock homolog (mouse)	2.7
Mylk	myosin light chain kinase	2.7
Crip1	cysteine-rich protein 1 (intestinal)	2.7
Plxdc2	plexin domain containing 2	2.7
Zmym1	zinc finger, MYM-type 1	2.7
Ptgs1	prostaglandin-endoperoxide synthase 1	2.7
Erbb3	v-erb-b2 erythroblastic leukemia viral oncogene homolog 3 (avian)	2.7
Pla1a	phospholipase A1 member A	2.6
Ptpn21	protein tyrosine phosphatase, non-receptor type 21	2.6

Supplementary Table S1 *(continued)*

Gene Symbol	Description	Fold Change (log2)
Hipk4	homeodomain interacting protein kinase 4	2.6
Ltbp2	latent transforming growth factor beta binding protein 2	2.6
Ltbp4	latent transforming growth factor beta binding protein 4	2.6
Sulf1	sulfatase 1	2.6
Prg4	proteoglycan 4	2.6
Ano6	anoctamin 6	2.6
Fam163a	family with sequence similarity 163, member A	2.5
Cpne9	copine family member IX	2.5
Zfp709l2	zinc finger protein 709-like 2	2.5
Arhgef19	Rho guanine nucleotide exchange factor (GEF) 19	2.5
Sema3b	Semaphorin 3B	2.5
Tnfrsf9	tumor necrosis factor receptor superfamily, member 9	2.5
Gem	GTP binding protein (gene overexpressed in skeletal muscle)	2.5
Zfp775	zinc finger protein 775	2.5
Zbtb45	zinc finger and BTB domain containing 45	2.4
Rcan1	regulator of calcineurin 1	2.4
Got1	glutamic-oxaloacetic transaminase 1, soluble (aspartate aminotransferase 1)	2.3
Def6	differentially expressed in FDCP 6 homolog (mouse)	2.3
Vps13a	vacuolar protein sorting 13 homolog A (S. cerevisiae)	2.2
Des	desmin	2.2
Osbp2	oxysterol binding protein 2	2.2
Vstm4	V-set and transmembrane domain containing 4	2.2
Crtc2	CREB regulated transcription coactivator 2	2.2

Supplementary Table S2 *List of genes with higher expression in Deeper AC than in the SFZ (ranks lower than 20th, fold change (log2) > 2)*

Gene Symbol	Description	Fold Change (log2)
Olr397	olfactory receptor 397	22.8
Alpl	alkaline phosphatase, liver/bone/kidney	22.5
Batf	basic leucine zipper transcription factor, ATF-like	22.4
Cks2	CDC28 protein kinase regulatory subunit 2	22.4
Tas2r120	taste receptor, type 2, member 120	22.1
Timp4	tissue inhibitor of metalloproteinase 4	22.0
Lysmd3	LysM, putative peptidoglycan-binding, domain containing 3	21.3
Mmp23	matrix metallopeptidase 23	20.1
Gmip	Gem-interacting protein	19.8
Klhl38	kelch-like 38 (Drosophila)	19.5
Foxa2	forkhead box A2	19.4
Fam111a	family with sequence similarity 111, member A	19.3
Zfp507	zinc finger protein 507	19.2
Tecta	tectorin alpha	19.2
Adam4l1	a disintegrin and metallopeptidase domain 4-like 1	19.0
Kcna1	potassium voltage-gated channel, shaker-related subfamily, member 1	18.6
Tsga13	testis specific, 13	18.5
Ivns1abp	influenza virus NS1A binding protein	18.2
Amhr2	anti-Mullerian hormone receptor, type II	17.7
Nsdhl	NAD(P) dependent steroid dehydrogenase-like	17.7
Mmp13	matrix metallopeptidase 13	17.4
Sox13	SRY (sex determining region Y)-box 13	17.3
Kcnk1	potassium channel, subfamily K, member 1	17.1
Slc6a1	solute carrier family 6 (neurotransmitter transporter, GABA), member 1	17.1
Ssx2ip	synovial sarcoma, X breakpoint 2 interacting protein	17.1
Dnm3	dynamin 3	17.1
SEPT1	NudC domain containing 1	16.9
Hsd17b13	hydroxysteroid (17-beta) dehydrogenase 13	16.9
Akr1c19	aldo-keto reductase family 1, member C19	16.9
Tpbg	trophoblast glycoprotein	16.6
Syt8	synaptotagmin VIII	16.5
Sphk1	sphingosine kinase 1	16.4
Odz3	odz, odd Oz/ten-m homolog 3 (Drosophila)	16.2
Kcnk6	potassium channel, subfamily K, member 6	15.9
Csrp2	cysteine and glycine-rich protein 2	15.9
Hoxa13	homeo box A13	15.6
Echdc2	enoyl CoA hydratase domain containing 2	15.5
Pcdha5	protocadherin alpha 5	15.3
SEPT11	hyaluronan and proteoglycan link protein 4	15.0
Rhbdl2	rhomboid, veinlet-like 2 (Drosophila)	15.0

Supplementary Table S2 *(continued)*

Gene Symbol	Description	Fold Change (log2)
Chd1	chromodomain helicase DNA binding protein 1	15.0
Tfr2	transferrin receptor 2	14.8
Abhd3	abhydrolase domain containing 3	14.7
LOC100125362	hypothetical protein LOC100125362	14.6
Vcpip1	valosin containing protein (p97)/p47 complex interacting protein 1	14.6
RGD1306941	similar to CG31122-PA	14.4
Art3	ADP-ribosyltransferase 3	14.3
Slc19a2	solute carrier family 19 (thiamine transporter), member 2	14.3
Mcc	mutated in colorectal cancers	14.1
Hadh	hydroxyacyl-CoA dehydrogenase	14.1
Mybph	myosin binding protein H	14.1
Tmem132e	transmembrane protein 132E	14.1
Wwtr1	WW domain containing transcription regulator 1	13.9
Cdv3	carnitine deficiency-associated gene expressed in ventricle 3 homolog (mouse)	13.8
Dact3	dapper, antagonist of beta-catenin, homolog 3 (Xenopus laevis)	13.7
Slc10a7	solute carrier family 10, member 7	13.6
Eln	elastin	13.6
Fkbpl	FK506 binding protein-like	13.5
LOC688390	hypothetical protein LOC688390	13.4
Gstt1	glutathione S-transferase theta 1	13.4
Myom1	myomesin 1	13.4
Wdr53	WD repeat domain 53	13.3
Prelid2	PRELI domain containing 2	13.2
Ppp1r14c	protein phosphatase 1, regulatory (inhibitor) subunit 14c	13.1
Fam70b	family with sequence similarity 70, member B	13.1
Plk5	polo-like kinase 5	13.0
Pcdh18	protocadherin 18	12.9
Wasf2	WAS protein family, member 2	12.9
Tfpi	tissue factor pathway inhibitor	12.8
Irf5	interferon regulatory factor 5	12.8
Kcnk2	potassium channel, subfamily K, member 2	12.7
Fmo4	flavin containing monooxygenase 4	12.5
Olr1014	olfactory receptor 1014	12.4
Ndrg4	N-myc downstream regulated gene 4	12.4
Arhgdig	Rho GDP dissociation inhibitor (GDI) gamma	12.1
Pnkp	polynucleotide kinase 3'-phosphatase	12.1
Fgfr3	fibroblast growth factor receptor 3	12.0
Masp1	mannan-binding lectin serine peptidase 1	12.0
Mtpn	myotrophin	12.0
Anpep	alanyl (membrane) aminopeptidase	12.0
Parva	parvin, alpha	11.9
Fbp1	fructose-1,6-bisphosphatase 1	11.9
LOC688459	hypothetical protein LOC688459	11.9
Zfp689	zinc finger protein 689	11.8
Rnase10	ribonuclease, RNase A family, 10 (non-active)	11.7
Pdpr	pyruvate dehydrogenase phosphatase regulatory subunit	11.7
Igflr1	IGF-like family receptor 1	11.7
Ina	internexin neuronal intermediate filament protein, alpha	11.7
Ccrn4l	CCR4 carbon catabolite repression 4-like (S. cerevisiae)	11.4
Serinc2	serine incorporator 2	11.4

Supplementary Table S2 *(continued)*

Gene Symbol	Description	Fold Change (log2)
Nat1	N-acetyltransferase 1	11.4
SEPT5	PYD and CARD domain containing	11.3
Gpr22	G protein-coupled receptor 22	11.2
Snrnp70	small nuclear ribonucleoprotein 70 (U1)	11.2
Tbccd1	TBCC domain containing 1	11.2
Dnah1	dynein, axonemal, heavy chain 1	11.2
RGD1565983	similar to apurinic/apyrimidinic endonuclease 2	11.1
Kctd4	potassium channel tetramerisation domain containing 4	11.1
Gpr171	G protein-coupled receptor 171	11.0
Zfp444	zinc finger protein 444	10.9
Pik3cb	phosphoinositide-3-kinase, catalytic, beta polypeptide	10.9
Hlx	H2.0-like homeobox	10.9
Nrsn2	neurensin 2	10.9
Pgm3	phosphoglucomutase 3	10.8
Lcmt2	leucine carboxyl methyltransferase 2	10.8
Trim43a	tripartite motif-containing 43A	10.8
Klf11	Kruppel-like factor 11	10.8
Eid3	EP300 interacting inhibitor of differentiation 3	10.8
RGD1562673	similar to Prostatic spermine-binding protein precursor (SBP)	10.8
Cd248	CD248 molecule, endosialin	10.7
Capn3	calpain 3	10.7
MARCH1	kelch-like 25 (Drosophila)	10.7
SEPT7	calreticulin 3	10.6
S1pr5	sphingosine-1-phosphate receptor 5	10.6
Rrad	Ras-related associated with diabetes	10.6
Vill	villin-like	10.6
Fads1	fatty acid desaturase 1	10.6
Irf6	interferon regulatory factor 6	10.5
Dync1li1	dynein cytoplasmic 1 light intermediate chain 1	10.4
Skap2	src kinase associated phosphoprotein 2	10.4
Cd2ap	CD2-associated protein	10.4
Clip2	CAP-GLY domain containing linker protein 2	10.4
Pglyrp1	peptidoglycan recognition protein 1	10.3
Bcas1	breast carcinoma amplified sequence 1	10.2
Fam117a	family with sequence similarity 117, member A	10.2
Cntf	ciliary neurotrophic factor	10.2
Paox	polyamine oxidase (exo-N4-amino)	10.2
Nagpa	N-acetylglucosamine-1-phosphodiester alpha-N-acetylglucosaminidase	10.2
C2	complement component 2	10.2
RGD1312026	similar to RIKEN cDNA C230081A13	10.1
Tuft1	tuftelin 1	10.1
Acbd5	acyl-CoA binding domain containing 5	10.1
Arhgap24	Rho GTPase activating protein 24	10.0
Myo1e	myosin IE	9.9
Slc22a18	solute carrier family 22, member 18	9.9
Gpr68	G protein-coupled receptor 68	9.8
Abhd10	abhydrolase domain containing 10	9.7
Il17re	interleukin 17 receptor E	9.7
Tfdp2	transcription factor Dp-2 (E2F dimerization partner 2)	9.7
Zfp800	zinc finger protein 800	9.7

Supplementary Table S2 *(continued)*

Gene Symbol	Description	Fold Change (log2)
Fgfr1	Fibroblast growth factor receptor 1	9.6
Slc29a2	solute carrier family 29 (nucleoside transporters), member 2	9.6
MARCH4	DnaJ (Hsp40) homolog, subfamily C, member 5 gamma	9.6
Pcdha13	protocadherin alpha 13	9.5
Taok1	TAO kinase 1	9.5
Prmt7	protein arginine methyltransferase 7	9.5
Cpeb4	cytoplasmic polyadenylation element binding protein 4	9.5
Pof1b	premature ovarian failure 1B	9.4
MARCH7	major facilitator superfamily domain containing 9	9.4
Crlf1	cytokine receptor-like factor 1	9.3
Pole2	polymerase (DNA directed), epsilon 2 (p59 subunit)	9.3
Ankrd23	ankyrin repeat domain 23	9.3
RGD1359634	similar to RIKEN cDNA 1700088E04	9.2
Mms22l	MMS22-like, DNA repair protein	9.1
Ppm1l	protein phosphatase, Mg2+/Mn2+ dependent, 1L	9.1
Sh3bp2	SH3-domain binding protein 2	9.1
SEPT3	ferredoxin-fold anticodon binding domain containing 1	9.0
Spata2L	spermatogenesis associated 2-like	9.0
Mal	mal, T-cell differentiation protein	8.9
Matn3	*matrilin* 3	8.9
Zfp583	zinc finger protein 583	8.9
Letm2	leucine zipper-EF-hand containing transmembrane protein 2	8.9
Cdk1	cyclin-dependent kinase 1	8.8
Aspg	asparaginase homolog (S. cerevisiae)	8.8
Zhx3	zinc fingers and homeoboxes 3	8.8
Iqgap3	IQ motif containing GTPase activating protein 3	8.8
Gpr116	G protein-coupled receptor 116	8.7
Lrp4	low density lipoprotein receptor-related protein 4	8.7
Mug1	*murinoglobulin* 1	8.7
Mum1l1	melanoma associated antigen (mutated) 1-like 1	8.7
Zap70	zeta-chain (TCR) associated protein kinase	8.7
Tmie	transmembrane inner ear	8.7
Sorcs2	sortilin-related VPS10 domain containing receptor 2	8.7
Scgb1c1	secretoglobin, family 1C, member 1	8.6
Pdlim3	PDZ and LIM domain 3	8.6
Zfp112	zinc finger protein 112	8.5
Slc13a5	solute carrier family 13, member 5	8.5
Slk	STE20-like kinase (yeast)	8.5
Olr584	olfactory receptor 584	8.4
Shbg	sex hormone binding globulin	8.4
Slc12a1	solute carrier family 12, member 1	8.4
Mettl4	methyltransferase like 4	8.4
Fam13a	family with sequence similarity 13, member A	8.3
Fem1b	fem-1 homolog b (C. elegans)	8.3
Prkg2	protein kinase, cGMP-dependent, type II	8.3
Shq1	SHQ1 homolog (S. cerevisiae)	8.2
Cdc7	cell division cycle 7 homolog (S. cerevisiae)	8.2
Slc16a10	solute carrier family 16, member 10	8.2
Mecom	MDS1 and EVI1 complex locus	8.1
Bdh1	3-hydroxybutyrate dehydrogenase, type 1	8.1

Supplementary Table S2 *(continued)*

Gene Symbol	Description	Fold Change (log2)
Gap43	growth associated protein 43	8.1
Cpamd8	C3 and PZP-like, alpha-2-macroglobulin domain containing 8	8.1
Rnf11	ring finger protein 11	8.0
Kif12	kinesin family member 12	8.0
Slc4a8	solute carrier family 4, sodium bicarbonate cotransporter, member 8	8.0
Rhobtb2	Rho-related BTB domain containing 2	8.0
Ren	renin	8.0
Fpgt	fucose-1-phosphate guanylyltransferase	8.0
Slc25a45	solute carrier family 25, member 45	8.0
Olr1229	olfactory receptor 1229	7.9
Apc2	adenomatosis polyposis coli 2	7.9
Ing5	inhibitor of growth family, member 5	7.9
Cnksr1	connector enhancer of kinase suppressor of Ras 1	7.9
Gngt2	G protein, gamma transducing activity polypeptide 2	7.8
Uggt1	UDP-glucose glycoprotein glucosyltransferase 1	7.8
Cryab	crystallin, alpha B	7.8
Ang	angiogenin, ribonuclease, RNase A family, 5	7.8
Trex2	three prime repair exonuclease 2	7.8
Zfp295	zinc finger protein 295	7.8
Polrmt	polymerase (RNA) mitochondrial (DNA directed)	7.8
Dnal1	dynein, axonemal, light chain 1	7.8
C1qtnf4	C1q and tumor necrosis factor related protein 4	7.8
Kif26b	kinesin family member 26B	7.7
Hebp1	heme binding protein 1	7.7
Mfn1	mitofusin 1	7.7
Man2a2	mannosidase 2, alpha 2	7.7
Opn3	opsin 3	7.7
Dsn1	DSN1, MIND kinetochore complex component, homolog (S. cerevisiae)	7.6
Npl	N-acetylneuraminate pyruvate lyase	7.6
Lsr	lipolysis stimulated lipoprotein receptor	7.6
Syndig1	synapse differentiation inducing 1	7.6
Nos1ap	nitric oxide synthase 1 (neuronal) adaptor protein	7.6
Cbln2	cerebellin 2 precursor	7.6
Catsper3	cation channel, sperm associated 3	7.5
Snn	stannin	7.5
Rasa2	RAS p21 protein activator 2	7.5
Wipi2	WD repeat domain, phosphoinositide interacting 2	7.5
Arl5a	ADP-ribosylation factor-like 5A	7.5
P2rx3	purinergic receptor P2X, ligand-gated ion channel, 3	7.5
Tmem132a	transmembrane protein 132A	7.5
Hif1an	hypoxia-inducible factor 1, alpha subunit inhibitor	7.4
Akr1c13	aldo-keto reductase family 1, member C13	7.4
Cav3	caveolin 3	7.4
Ppp1r3b	protein phosphatase 1, regulatory subunit 3B	7.4
Dync2li1	dynein cytoplasmic 2 light intermediate chain 1	7.4
Sord	sorbitol dehydrogenase	7.4
Otud3	OTU domain containing 3	7.4
Car6	carbonic anhydrase 6	7.3
Radil	Ras association and DIL domains	7.3
Layn	layilin	7.3

Supplementary Table S2 *(continued)*

Gene Symbol	Description	Fold Change (log2)
Tacc3	transforming, acidic coiled-coil containing protein 3	7.3
Grhl3	grainyhead-like 3 (Drosophila)	7.3
Elf1	E74-like factor 1	7.3
Lrrc4c	leucine rich repeat containing 4C	7.3
Vps4a	vacuolar protein sorting 4 homolog A (S. cerevisiae)	7.2
Mast3	microtubule associated serine/threonine kinase 3	7.2
RGD1307621	hypothetical LOC314168	7.2
Entpd5	ectonucleoside triphosphate diphosphohydrolase 5	7.2
Pde3b	phosphodiesterase 3B, cGMP-inhibited	7.2
Myh11	myosin, heavy chain 11, smooth muscle	7.1
Synpr	synaptoporin	7.1
Cdc20	cell division cycle 20 homolog (S. cerevisiae)	7.1
Galnt4	GalNAc-T4	7.1
LOC100188933	hypothetical protein LOC100188933	7.1
Meox2	mesenchyme homeobox 2	7.1
Krt19	keratin 19	7.1
Ints12	integrator complex subunit 12	7.1
RGD1564854	similar to divalent cation tolerant protein CUTA	7.1
Tmem125	transmembrane protein 125	7.1
Scara5	scavenger receptor class A, member 5 (putative)	7.0
Tmem81	transmembrane protein 81	7.0
Bcar3	breast cancer anti-estrogen resistance 3	7.0
Mypn	myopalladin	6.9
Cetn4	centrin 4	6.9
Spc25	SPC25, NDC80 kinetochore complex component, homolog (S. cerevisiae)	6.9
Atf7	activating transcription factor 7	6.9
Slc30a9	solute carrier family 30 (zinc transporter), member 9	6.9
Zic4	Zic family member 4	6.9
Galntl1	galactosamine:polypeptide N-acetylgalactosaminyltransferase-like 1	6.9
Pigw	phosphatidylinositol glycan anchor biosynthesis, class W	6.9
Gstm5	glutathione S-transferase, mu 5	6.9
Dd25	hypothetical protein Dd25	6.9
St14	suppression of tumorigenicity 14 (colon carcinoma)	6.9
RGD1305014	similar to RIKEN cDNA 2310057M21	6.8
Apbb1ip	A4 precursor protein-binding, family B, member 1 interacting protein	6.8
Haus3	HAUS augmin-like complex, subunit 3	6.8
Serpinf2	serpin peptidase inhibitor, clade F, member 2	6.8
Psmb9	proteasome (prosome, macropain) subunit, beta type 9	6.8
Rsph9	radial spoke head 9 homolog (Chlamydomonas)	6.8
Pvrl2	poliovirus receptor-related 2	6.8
Slc39a8	solute carrier family 39 (zinc transporter), member 8	6.8
Adam4	a disintegrin and metalloprotease domain 4	6.8
Akr1c2	aldo-keto reductase family 1, member C2	6.8
Galntl6	galactosamine:polypeptide N-acetylgalactosaminyltransferase-like 6	6.8
Nedd4l	neural precursor cell expressed, developmentally down-regulated 4-like	6.7
Syncrip	synaptotagmin binding, cytoplasmic RNA interacting protein	6.7
Hyal6	hyaluronoglucosaminidase 6	6.7
Bend6	BEN domain containing 6	6.7
Spag4	sperm associated antigen 4	6.6
Cx3cl1	chemokine (C-X3-C motif) ligand 1	6.6